A&A 417, 1173–1181 (2004)
DOI: 10.1051/0004-6361:20034174

Astronomy & Astrophysics

Dielectronic recombination data for dynamic finite-density plasmas

IV. The carbon isoelectronic sequence

O. Zatsarinny[1], T. W. Gorczyca[1], K. T. Korista[1], N. R. Badnell[2], and D. W. Savin[3]

[1] Department of Physics, Western Michigan University, Kalamazoo, Michigan 49008, USA
e-mail: oleg.zatsarinny;korista@wmich.edu
[2] Department of Physics, University of Strathclyde, Glasgow, G4 0NG, UK
[3] Columbia Astrophysics Laboratory, Columbia University, New York, NY 10027, USA
e-mail: savin@astro.columbia.edu

Received 8 August 2003 / Accepted 18 December 2003

Abstract. Dielectronic recombination (DR) and radiative recombination (RR) data for carbon-like ions forming nitrogen-like ions have been calculated as part of the assembly of a level-resolved DR and RR database necessary for modelling of dynamic finite-density plasmas (Badnell et al. 2003). Total DR and RR rate coefficients are presented and the results discussed for N^{+} to Zn^{24+}, as well as Kr^{30+}, Mo^{36+}, Cd^{42+}, and Xe^{48+}. We find that the $2 \rightarrow 2$ (no change in the principal quantum number of the core electron) low-temperature DR does not scale smoothly with nuclear charge Z due to resonances straddling the ionization limit, thereby making explicit calculations for each ion necessary. The RR and DR data are suitable for modelling of solar and cosmic plasmas under conditions of collisional ionization equilibrium, photoionization equilibrium, and non-equilibrium ionization.

Key words. atomic data – atomic processes – plasmas

1. Introduction

Dielectronic recombination (DR) is an important recombination process for laboratory and astrophysical plasmas. Accurate DR rate coefficients are needed for determining the ionization balance of these plasmas and also for interpreting the spectra from most types of astrophysical and laboratory plasmas. While the DR process has been subject to intense theoretical study, the existing sophisticated calculations have usually only been performed for certain selected ions, and furthermore, most of the available data were computed using simplified theoretical models. Recently, a critical evaluation of the uncertainties of the existing theoretical DR rate coefficients has been performed by Savin & Laming (2002). It was found that near the temperatures of peak formation in collisional ionization equilibrium, for some ions the DR uncertainties can be as large as a factor of 2–5. Savin & Laming identified DR rate coefficients for carbon-like ions as one of the most urgent needs for solar and stellar applications. The overall uncertainty of the published DR rate coefficients for carbon-like ions has been estimated at ≈70%. Recent experimental measurements (Savin et al. 1997, 1999, 2002a,b, 2003) have also shown that many earlier DR calculations are not accurate and improved, systematic calculations are needed. Most of the earlier calculations neglected the contributions from the fine-structure $2p_{3/2} - 2p_{1/2}$ excitation, which has been shown to be very important for low-temperature DR rate coefficients (e.g., Savin et al. 1997, 1999, 2002a,b, 2003). Including fine-structure excitations is thus essential to produce reliable DR rate coefficients applicable for modelling photoionized plasmas where low-temperature DR plays an important role.

Our program is designed to generate a reliable level-resolved DR database necessary for spectroscopic modelling of plasmas in ionization equilibrium and non-equilibrium, as has been described by Badnell et al. (2003), Zatsarinny et al. (2003), and Colgan et al. (2003). The database includes total and final-state level-resolved results from both the ground and metastable states of the C-like target ion. The final-state resolved results are important for the collisional-radiative modelling of dense plasmas and the results from metastable states are required for modelling dynamic plasmas – plasmas whose excited states are not all in quasi-static equilibrium with the ground state. Calculations have been carried out in intermediate coupling to produce DR data for the isoelectronic sequences of all first and second row elements (and selected other elements). In this paper, we describe calculations and results of DR data for carbon-like ions forming nitrogen-like ions. Ions from the carbon-like isoelectronic sequence are found in

Send offprint requests to: T. W. Gorczyca,
e-mail: gorczyca@wmich.edu

photoionized environments, as well as in high temperature collisionally ionized gases. This sequence has also been shown to be important in the astrophysical modelling of X-ray photoionized gas (Savin et al. 1999), and in the determination of solar and stellar upper atmosphere abundances (Savin & Laming 2002). Although a few studies for separate elements of this sequence have been made, there are no systematic data on DR rate coefficients for the entire carbon-like sequence.

LS-coupling results were first presented for the C, N, O, Ne, Mg, Si, S, Ca, Fe, and Ni *isonuclear* ions by Jacobs et al. (1977, 1978, 1979, 1980). They used a simplified model where the autoionization rates are obtained from the threshold values of the partial-wave electron-impact excitation cross sections for the corresponding ions, and radiative decay of autoionizing states was approximated as the ionic core radiative decay rate. Comparison with the latest experimental and theoretical data shows that this simplified model can significantly underestimate DR rate coefficients at low temperatures (Savin et al. 1997, 1999, 2002a,b, 2003; Zatsarinny et al. 2003).

The first study of the intermediate-coupling (IC) effects in the DR of carbon-like ions was performed by Badnell & Pindzola (1989). Their high-temperature IC results for carbon-like O^{2+} were no more than 5% greater than the LS-coupling results. This small IC enhancement in DR rate coefficients was explained by the fact that the LS-forbidden high-n resonances were not as important an additional contribution to the DR rate coefficients as they are in other systems. However, Badnell & Pindzola (1989) did not include the contributions from the fine-structure $2p_{3/2} - 2p_{1/2}$ excitation. Thus, their low-temperature DR rate coefficient lacks other IC effects.

All of the available theoretical DR data for carbon-like ions from N^+ to Ni^{22+} were reviewed and fitted by Mazzotta et al. (1998). Since that review, calculations for DR plus RR of low-charged N^+ and O^{2+} were performed by Nahar & Pradhan (1997) and Nahar (1999), respectively, using an LS-coupled R-matrix approach. The total recombination rate coefficients computed by Nahar & Pradhan (1997) and Nahar (1999) are lower than the results which were reviewed and fitted by Mazzotta et al. (1998) by ≈20% in the high-temperature region.

Precise experimental measurements for carbon-like Fe^{20+} have been performed recently by Savin et al. (2003) for DR via $N = 2 \rightarrow N' = 2$ core excitation, using the heavy-ion Test Storage Ring (TSR) in Heidelberg, Germany. Here N is the principal quantum number of the core electron. The cooler electrons employed in this technique allowed resolution of separate resonances and their fine structure components. Significant discrepancies were found between experimentally derived rate coefficients and previously published theoretical results, especially in the low-temperature region. Hence, the measurements call into question all previous theoretical $2 \rightarrow 2$ DR rate coefficients used for ionization balance calculations of cosmic plasmas. In the work of Savin et al. (1997, 1999, 2002a,b, 2003), new theoretical calculations were also carried out using intermediate-coupling multiconfiguration Breit-Pauli (MCBP) and multiconfiguration Dirac-Fock (MCDF) approaches as well as the R-matrix method, the Hebrew University Lawrence Livermore Atomic Code (HULLAC) and the Flexible Atomic Code (FAC). Details of these calculations are discussed in Savin (2002b, 2003). These new theoretical results yield good agreement with experiment.

In this paper, we apply a similar intermediate-coupling MCBP method, in the isolated resonance approximation, to compute DR rate coefficients for all carbon-like ions from N^+ to Zn^{24+}, and also for the highly-charged ions Kr^{30+}, Mo^{36+}, Cd^{42+} and Xe^{48+}. The rate coefficients reported here cover a wide range of temperatures and ionic species, and are expected to be as accurate as any results to date; the very recent results of Gu (2003) we consider to be at the same level of accuracy as ours, as demonstrated below.

In the present calculations, we produce final-state level-resolved DR rate coefficients, from both the ground and metastable states, as well as totals. Total DR rate coefficients (along with total RR rate coefficients) are presented in compact form using simple fitting formulae. Data are presented for each ion, since the large irregularity in Z-dependence of the total DR rate coefficients at low temperatures makes scaling inaccurate. It is impractical to list all level-resolved rate coefficients in a paper publication. As previously discussed (Badnell et al. 2003), the present data will form part of an Atomic Data and Analysis Structure (ADAS) dataset comprising the *adf09* files for each ion, detailing the rate coefficients to each LSJ-resolved final state. This is available through the ADAS project (Summers 2003), and is also made available online at the Oak Ridge Controlled Fusion Atomic Data Center (`http://www-cfadc.phy.ornl.gov/data_and_codes`).

The rest of this paper is organized as follows: in Sect. 2, we give a brief description of the theory used and the details of our calculations for the carbon-like ions. In Sect. 3, we present results for the total DR rate coefficients for 28 ions in this sequence. We conclude with a brief summary in Sect. 4.

2. Theory

Details of our calculations have already been described elsewhere (Badnell et al. 2003; Zatsarinny et al. 2003). Here we outline only the main points. DR cross section calculations were carried out using the code AUTOSTRUCTURE (Badnell 1986; Badnell & Pindzola 1989) which is based on lowest order perturbation theory, where both the electron-electron and electron-photon interactions are treated to first order. This independent-processes, isolated-resonance approximation is used to calculate configuration-mixed LS and IC energy levels, radiative rates, and autoionization rates, which are then used to compute Lorentzian DR resonance profiles. This enables the generation of final state level-resolved and total DR rate coefficients.

The DR process for carbon-like ions of an arbitrary atom "A" can be represented, in intermediate coupling, as:

$$\begin{aligned} & e^- + A^{q+}\left(2s^2 2p^2\left[{}^3P_0\right]\right) \rightarrow \\ & \left\{\begin{array}{l} A^{(q-1)+}\left(2s^2 2p^2\left[{}^3P_{1,2};\ {}^1D_2;\ {}^1S_0\right] nl\right) \\ A^{(q-1)+}\left(2s2p^3\left[{}^5S^o_2;\ {}^3D^o_{1,2,3};\ {}^3P^o_{0,1,2};\ {}^3S^o_1;\ {}^1D^o_2;\ {}^1P^o_1\right] nl\right) \\ A^{(q-1)+}\left(2p^4\left[{}^3P_{0,1,2};\ {}^1D_2;\ {}^1S_0\right] nl\right). \end{array}\right\} \\ & \rightarrow A^{(q-1)+} + h\nu \end{aligned} \quad (1)$$

for $2 \rightarrow 2$ core excitation, where we included all $0 \le l \le 15$ and $n_{\rm min} \le n \le 1000$ ($n_{\rm min}$ is the lowest autoionizing state, which varies from $n_{\rm min} = 3$ for N^+ to $n_{\rm min} = 6$ for Xe^{48+}). For $2 \rightarrow 3$ excitation, the DR process can be written as

$$e^- + A^{q+}\left(2s^2 2p^2\left[^3P_0\right]\right) \rightarrow \left\{\begin{array}{l} A^{(q-1)+}\left(2s^2 2p 3lnl'\right) \\ A^{(q-1)+}\left(2s 2p^2 3lnl'\right) \\ A^{(q-1)+}\left(2p^3 3lnl'\right) \end{array}\right\} \rightarrow A^{(q-1)+} + h\nu \quad (2)$$

with $0 \le l \le 6$ and $3 \le n \le 1000$ (the contribution due to higher-l DR drops off faster in this case).

A bound orbital basis (1s, 2s, 2p, 3s, 3p, 3d) was generated from a configuration-average Hartree-Fock (Froese Fischer 1991) calculation for the $1s^2 2s^2 2p^2$ configuration to get the first three orbitals, followed by a configuration-average, frozen-core HF calculation for the $1s^2 2s^2 2p 3l$ states to get the additional $n = 3$ orbitals. Then the corresponding atomic structure for the initial ionic states, the intermediate resonance states, and the final recombined bound states were obtained by diagonalizing the appropriate Breit-Pauli Hamiltonians. All target states were obtained with full configuration and spin-orbit mixing of configurations indicated in Eqs. (1) and (2). Prior to the final DR calculations, the ionic thresholds were shifted to the known spectroscopic values (`http://physics.nist.gov/cgi-bin/AtData/main_asd`) by a small amount – typically in the range of 1–2 eV for high Z. Distorted wave calculations were then performed to generate the appropriate free εl and bound nl ($n > 3$) orbitals which are attached to each target state to yield the continuum and resonance states, respectively. All of the above orbitals are computed in the absence of any relativistic effects. However, the continuum and resonance states are subsequently recoupled to an intermediate coupling scheme in order to include relativistic effects to lowest order. Also, the DR contribution from $3l3l'$ autoionizing states is considered separately with full configuration and spin-orbit mixing between these states.

The DR data is a sum of Lorentzian profiles and can therefore be convoluted analytically with the experimental energy distribution, in order to compare to measured results, or with a Maxwellian electron distribution, in order to obtain total DR rate coefficients. This represents a huge savings in computational effort over R-matrix calculations since the latter must be performed for an extremely dense mesh in order to fully resolve all resonances (Gorczyca et al. 2002; Ramirez & Bautista 2002). The total DR rate coefficients were then fitted as

$$\alpha_{\rm DR}(T) = T^{-3/2} \sum_i c_i e^{-E_i/T} \quad (3)$$

in order to facilitate the further application of our data. Here, the electron temperature T and the energy fitting parameter E_i are in units of eV, and the rate coefficient $\alpha_{\rm DR}(T)$ is in units of 10^{-11} cm^3 s^{-1}. Table 1 lists the fitting parameters c_i and E_i for each member of the carbon-like sequence treated. The fits are accurate to within a maximum difference of 3% for 0.001 eV $< T <$ 100 000 eV. This covers the temperature range over which the ions discussed in this paper are predicted to form in both photoionization equilibrium and collisional ionization equilibrium. Note that different parameters c_i and E_i in Table 1 reflect different recombination channels in Eqs. (1) and (2): Cols. 2–5 correspond to the $2p \rightarrow 2p$ core excitation in Eq. (1), Cols. 6 and 7 correspond to the $2s \rightarrow 2p$ core excitation in Eq. (1), and Cols. 8 and 9 correspond to the $2 \rightarrow 3$ ($n = 3$) and ($n > 3$) channels in Eq. (2), respectively.

In order to provide total (DR+RR) recombination rate coefficients, Table 1 also contains the fitting coefficients for the RR rate coefficients. These were also obtained using the AUTOSTRUCTURE code with the same target orbitals and in the same approximation as the DR calculations. RR rate coefficients were fitted with the formula of Verner & Ferland (1996),

$$\alpha_{\rm RR}(T) = a\left[\sqrt{T/T_0}\left(1 + \sqrt{T/T_0}\right)^{1-b}\left(1 + \sqrt{T/T_1}\right)^{1+b}\right]^{-1}, \quad (4)$$

where the fitting parameters T_0 and T_1 are in units of eV, a is in units of 10^{-11} cm^3 s^{-1}, and b is dimensionless. This form ensures the correct asymptotic behavior of the RR rate coefficients for low and high temperatures: $\alpha_{\rm RR}(T) \propto T^{-1/2}$ at $T \ll T_0, T_1$, and $\alpha_{\rm RR}(T) \propto T^{-3/2}$ at $T \gg T_0, T_1$. The average accuracy of the fitting is better than 4% in the range of temperatures from 10^{-5} eV to 10^{+5} eV (the error is still less than 8% for all ions at all temperatures).

AUTOSTRUCTURE is implemented within the ADAS suite of programs as ADAS701. It produces raw autoionization and radiative rates which must be post-processed to obtain the final-state level-resolved and total DR rate coefficients. The post-processor ADASDR is used to reorganize the resultant data and also to add in radiative transitions between highly-excited Rydberg states, which are computed hydrogenically. This post-processor outputs directly the *adf09* file necessary for use by ADAS. The *adf09* files generated by our calculations in the IC configuration mixed approximations are available electronically (`http://www-cfadc.phy.ornl.gov/data_and_codes`). This site has tabulated DR rate coefficients into final LSJ levels from both the ground and metastable states in a manner useful to fusion and astrophysical modelers. Separate files *adf09* are produced for the excitations $2 \rightarrow 2$, $2 \rightarrow 3$ (capture to $n = 3$), and $2 \rightarrow 3$ (capture to $n > 3$), which are thus amenable to selective upgrade.

3. Results

Because of the complexity of the theoretical description for the DR process, it is almost impossible to say a priori which approximations in the calculations are justified and which are not. Laboratory measurements are needed to ensure that even state-of-the-art techniques produce reliable results. Before carrying out the systematic calculations for DR rate coefficients for a whole sequence, we therefore first checked the chosen approximations by comparing to the available experimental data. Figure 1 presents the comparison of our calculations of DR rate coefficients with results of measurements using the heavy-ion TSR in Heidelberg (Savin et al. 2003) for Fe^{20+} to Fe^{19+} recombination. The cooler electrons employed in this technique have an anisotropic Maxwellian distribution with low

Table 1. Fitting coefficients of Eqs. (3) and (4) for dielectronic and radiative recombination of C-like ions forming N-like ions: Cols. 2–5 correspond to 2p → 2p DR, Cols. 6 and 7 correspond to 2s → 2p DR, Col. 8 to 2 → 3 (n = 3) DR, Col. 9 to 2 → 3 (n > 0) DR, and Cols. 10 and 11 to the calculated RR rate coefficients. The c_i and a are in units of 10^{-11} cm^3 s^{-1}, the E_i, T_0, and T_1 are in eV, and b is dimensionless.

Ion	c_1	c_2	c_3	c_4	c_5	c_6	c_7	c_8	a	b
N^{+}	2.678E-02	1.614E-02	7.742E-02	0.000E+00	2.182E+00	8.809E+01	9.754E-01	3.906E+00	2.522E+01	7.282E-01
O^{2+}	4.223E-02	1.879E-02	5.227E-02	0.000E+00	8.415E+00	3.113E+02	6.300E+00	2.885E+01	3.831E+02	8.293E-01
F^{3+}	3.834E-01	7.290E-02	4.560E-02	6.087E-01	3.239E+01	5.162E+02	1.347E+01	1.682E+02	8.136E+02	8.578E-01
Ne^{4+}	1.273E-01	1.954E-01	1.023E+00	2.605E+00	3.084E+01	8.834E+02	7.273E+01	6.109E+02	9.087E+02	8.639E-01
Na^{5+}	2.941E-01	5.618E-01	1.548E+00	8.962E+00	1.484E+02	1.748E+03	1.347E+02	1.417E+03	7.544E+02	8.617E-01
Mg^{6+}	2.637E-01	2.615E+00	3.353E+00	8.588E+00	5.903E+01	1.891E+03	2.590E+02	2.941E+03	6.342E+02	8.563E-01
Al^{7+}	3.931E-01	8.492E+00	5.079E+00	5.555E+00	6.221E+01	1.651E+03	5.041E+02	5.066E+03	5.758E+02	8.507E-01
Si^{8+}	2.648E-01	1.097E+01	4.828E+01	3.996E+01	1.089E+02	2.358E+03	9.014E+02	8.237E+03	5.544E+02	8.459E-01
P^{9+}	1.091E+00	4.121E+00	9.368E+00	4.007E+01	1.855E+02	2.867E+03	1.496E+03	1.218E+04	5.446E+02	8.416E-01
S^{10+}	9.451E-01	1.998E+00	1.138E+01	2.457E+01	2.049E+02	2.986E+03	2.140E+03	1.688E+04	5.276E+02	8.365E-01
Cl^{11+}	5.080E+00	8.663E+00	3.229E+01	3.397E+02	3.924E+02	1.389E+04	2.804E+03	2.263E+04	5.189E+02	8.311E-01
Ar^{12+}	3.988E+00	5.400E+00	2.595E+01	6.056E+01	2.951E+02	3.648E+03	3.704E+03	2.897E+04	5.338E+02	8.286E-01
K^{13+}	5.296E-01	2.195E+01	1.465E+01	2.050E+02	2.768E+02	4.332E+03	4.757E+03	3.599E+04	5.256E+02	8.243E-01
Ca^{14+}	6.210E+00	1.369E+01	6.372E+01	1.850E+02	5.378E+02	4.604E+03	5.978E+03	4.346E+04	5.163E+02	8.201E-01
Sc^{15+}	6.199E+00	1.551E+01	1.037E+02	3.987E+02	9.344E+02	4.684E+03	7.579E+03	5.092E+04	5.399E+02	8.188E-01
Ti^{16+}	7.147E+01	1.852E+01	9.129E+01	3.989E+02	5.154E+02	5.887E+03	9.216E+03	5.861E+04	5.608E+02	8.172E-01
V^{17+}	2.070E+01	1.525E+02	1.411E+02	7.921E+02	6.558E+02	6.188E+03	1.106E+04	6.707E+04	5.738E+02	8.152E-01
Cr^{18+}	6.463E+00	1.231E+01	6.521E+01	1.996E+02	1.032E+03	6.754E+03	1.367E+04	7.536E+04	5.849E+02	8.131E-01
Mn^{19+}	8.899E-01	1.027E+01	6.521E+01	2.363E+02	1.470E+03	7.000E+03	1.611E+04	8.331E+04	5.920E+02	8.109E-01
Fe^{20+}	1.706E+01	6.450E+01	1.120E+02	9.795E+02	1.278E+03	7.471E+03	1.837E+04	9.099E+04	5.947E+02	8.083E-01
Co^{21+}	0.000E+00	4.819E+01	1.135E+02	6.241E+02	1.739E+03	8.682E+03	2.144E+04	9.986E+04	6.021E+02	8.059E-01
Ni^{22+}	1.429E+00	1.156E+01	2.092E+02	1.394E+03	2.032E+03	8.458E+03	2.339E+04	1.086E+05	6.176E+02	8.047E-01
Cu^{23+}	1.529E+02	1.087E+01	1.095E+02	1.090E+03	1.966E+03	9.996E+03	2.721E+04	1.170E+05	6.275E+02	8.033E-01
Zn^{24+}	2.274E+01	3.120E+01	5.397E+01	1.361E+03	2.982E+03	1.101E+04	3.069E+04	1.269E+05	6.623E+02	8.036E-01
Kr^{30+}	1.352E+01	4.158E+01	1.036E+02	8.743E+02	5.588E+03	1.898E+04	5.275E+04	1.748E+05	7.398E+02	7.966E-01
Mo^{36+}	3.829E+01	2.874E+02	4.953E+02	1.859E+03	9.605E+03	3.038E+04	8.139E+04	2.210E+05	8.261E+02	7.917E-01
Cd^{42+}	3.354E+00	3.524E+02	2.015E+03	6.587E+03	5.075E+03	4.791E+04	1.051E+05	2.471E+05	8.929E+02	7.870E-01
Xe^{48+}	2.611E+02	0.000E+00	3.060E+02	1.253E+03	1.576E+04	6.743E+04	1.451E+05	2.636E+05	1.012E+03	7.863E-01
	E_1	E_2	E_3	E_4	E_5	E_6	E_7	E_8	T_0	T_1
N^{+}	6.280E-03	1.362E-02	1.820E-01	0.000E+00	5.818E+00	1.510E+01	1.836E+01	2.054E+01	2.460E-05	4.432E+00
O^{2+}	1.513E-02	2.719E-02	3.300E-01	0.000E+00	7.312E+00	1.954E+01	3.136E+01	3.429E+01	2.600E-06	2.237E+01
F^{3+}	8.800E-03	2.720E-02	1.000E-01	1.096E+00	1.029E+01	2.413E+01	4.749E+01	5.636E+01	3.000E-06	4.908E+01
Ne^{4+}	2.740E-02	5.690E-02	3.062E-01	1.130E+00	8.520E+00	2.766E+01	6.107E+01	7.901E+01	7.200E-06	8.431E+01
Na^{5+}	2.730E-02	6.630E-02	2.307E-01	1.945E+00	1.341E+01	3.392E+01	7.707E+01	1.045E+02	2.370E-05	1.282E+02
Mg^{6+}	3.040E-02	1.037E-01	2.644E-01	1.351E+00	7.380E+00	3.552E+01	9.243E+01	1.322E+02	6.550E-05	1.807E+02
Al^{7+}	1.134E-01	2.533E-01	5.949E-01	1.861E+00	5.565E+00	3.621E+01	1.071E+02	1.630E+02	1.413E-04	2.442E+02
Si^{8+}	6.290E-02	1.855E-01	4.342E-01	1.195E+00	9.168E+00	4.294E+01	1.206E+02	1.971E+02	2.524E-04	3.151E+02
P^{9+}	1.673E-01	3.504E-01	9.046E-01	2.713E+00	1.292E+01	4.681E+01	1.344E+02	2.333E+02	4.090E-04	3.945E+02
S^{10+}	2.210E-02	5.850E-02	2.231E-01	1.040E+00	6.848E+00	4.871E+01	1.513E+02	2.722E+02	6.496E-04	4.891E+02
Cl^{11+}	6.980E-02	1.541E-01	4.595E-01	1.317E+00	6.581E+00	5.459E+01	1.693E+02	3.148E+02	9.723E-04	5.946E+02
Ar^{12+}	2.250E-02	2.312E-01	5.682E-01	2.179E+00	1.062E+01	5.648E+01	1.864E+02	3.593E+02	1.284E-03	6.983E+02
K^{13+}	2.870E-02	9.540E-02	3.137E-01	1.565E+00	5.849E+00	5.845E+01	2.061E+02	4.059E+02	1.797E-03	8.229E+02
Ca^{14+}	1.839E-01	5.832E-01	1.571E+00	5.254E+00	1.691E+01	6.547E+01	2.263E+02	4.561E+02	2.470E-03	9.595E+02
Sc^{15+}	3.000E-02	2.899E-01	1.334E+00	3.616E+00	1.962E+01	7.701E+01	2.475E+02	5.079E+02	2.953E-03	1.086E+03
Ti^{16+}	6.500E-02	1.027E-01	2.918E-01	8.174E-01	4.731E+00	6.699E+01	2.697E+02	5.639E+02	3.519E-03	1.226E+03
V^{17+}	3.250E-02	2.102E-01	6.298E-01	1.875E+00	7.350E+00	6.989E+01	2.937E+02	6.220E+02	4.252E-03	1.382E+03
Cr^{18+}	3.570E-02	1.324E-01	2.863E-01	1.865E+00	7.589E+00	7.594E+01	3.172E+02	6.828E+02	5.106E-03	1.548E+03
Mn^{19+}	3.920E-02	1.096E-01	5.811E-01	1.719E+00	6.314E+00	6.110E+01	3.421E+02	7.460E+02	6.143E-03	1.724E+03
Fe^{20+}	1.592E-01	3.501E-01	9.926E-01	3.083E+00	1.017E+01	7.461E+01	3.674E+02	8.122E+02	7.420E-03	1.923E+03
Co^{21+}	0.000E+00	3.217E-01	5.982E-01	1.414E+00	8.310E+00	8.319E+01	3.951E+02	8.816E+02	8.751E-03	2.148E+03
Ni^{22+}	4.750E-02	4.900E-01	1.395E+00	6.183E+00	2.194E+01	1.086E+02	4.234E+02	9.523E+02	9.972E-03	2.340E+03
Cu^{23+}	5.000E-02	1.124E-01	1.075E+00	4.250E+00	1.164E+01	9.356E+01	4.539E+02	1.026E+03	1.148E-02	2.539E+03
Zn^{24+}	5.250E-02	1.637E-01	7.883E-01	3.522E+00	1.256E+01	9.568E+01	4.833E+02	1.103E+03	1.220E-02	2.739E+03
Kr^{30+}	8.420E-01	2.045E+00	1.259E+00	7.135E+00	2.243E+01	1.214E+02	6.983E+02	1.613E+03	2.341E-02	4.327E+03
Mo^{36+}	9.130E-01	1.760E+00	4.837E+00	1.258E+01	4.322E+01	1.806E+02	9.641E+02	2.223E+03	3.844E-02	6.033E+03
Cd^{42+}	6.186E-01	1.595E+00	4.767E+00	7.845E+00	4.158E+01	2.274E+02	1.317E+03	2.939E+03	6.032E-02	8.294E+03
Xe^{48+}	4.500E-01	0.000E+00	3.032E+00	5.756E+00	4.717E+01	3.080E+02	1.679E+03	3.804E+03	7.991E-02	1.078E+04

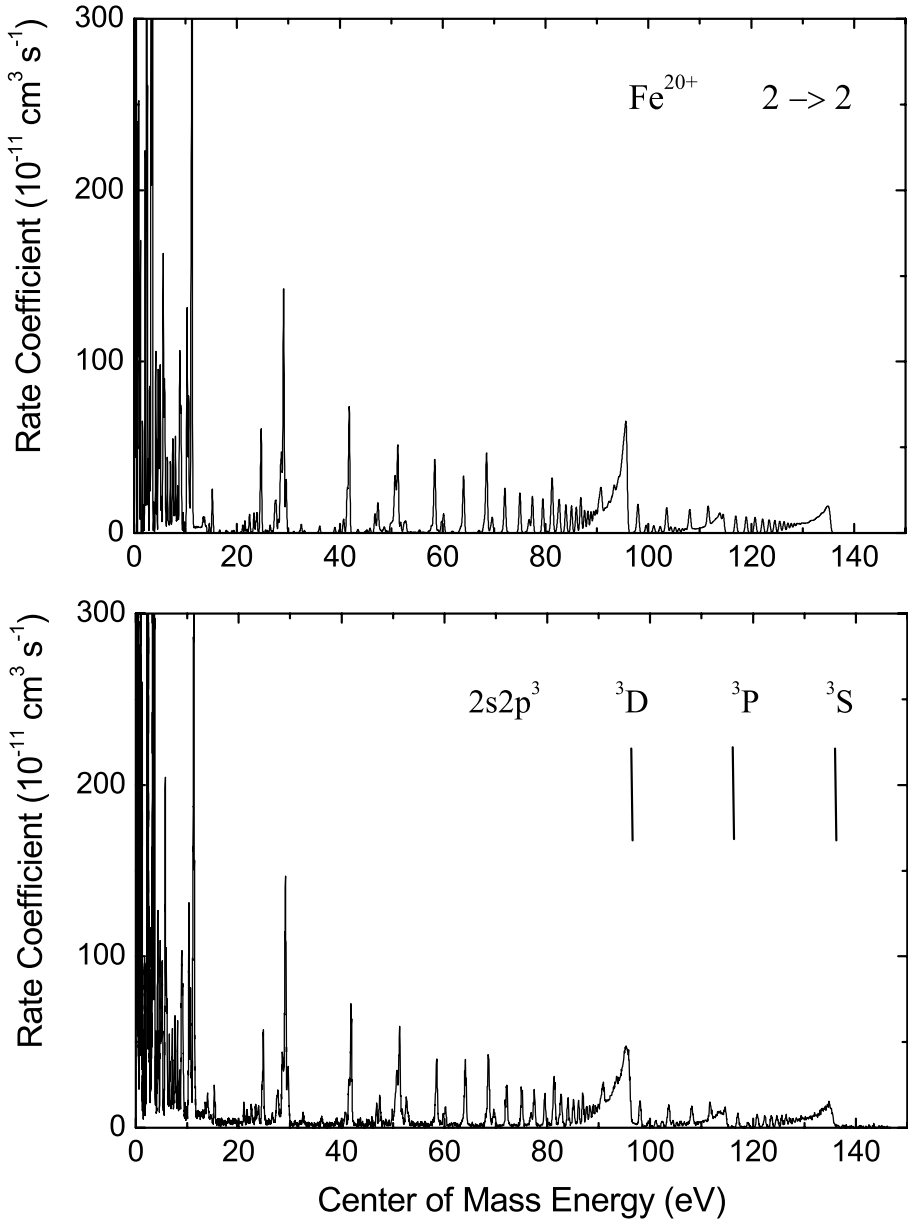

Fig. 1. Fe^{20+} to Fe^{19+} DR rate coefficients due to $2 \rightarrow 2$ core excitation: **a)** the present MCBP calculations convolved with the experimental energy spread of Savin et al. (2003); **b)** TSR experiment (Savin et al. 2003).

perpendicular and parallel temperatures of $k_BT_\perp \approx 15$ meV and $k_BT_\parallel \approx 0.15$ meV, and allow resolution of separated resonances associated with $2 \rightarrow 2$ core excitations. These measurements therefore allow a very detailed comparison for the DR process.

As seen in Fig. 1, our calculations based on the MCBP method in the isolated-resonance approximation reproduce all the main resonances and their intensities fairly well. The most notable discrepancies are for the low-energy resonances just above threshold. At higher energies, taking the ratio of the theoretical to experimental resonance strengths results in a 1σ scatter of ≈30%. Similar results were found for Fe^{19+} to Fe^{18+} DR for MCBP, MCDF, and HULLAC results (Savin et al. 2002b). This is larger than the estimated relative experimental uncertainty of 10% for comparing DR results at different energies. This ≈30% scatter provides an estimate for the accuracy of the level-resolved DR calculations for current state-of-the-art DR calculations.

As we see from Fig. 1, all dipole-allowed core transitions ($2s^22p^2 \rightarrow 2s2p^3$ ^3D, ^3P, ^3S) contribute significantly to the total DR process. Note also that the high-lying maximum at the $2s2p^3$ ^3S excitation threshold is almost fully due to a one-step cascade when the intermediate state radiates into autoionizing states which then radiatively stabilize.

The Maxwellian DR rate coefficients for Fe^{20+} as a function of electron temperature are compared in Fig. 2 with experimentally derived results and other published theoretical results. Also shown in Fig. 2 are the contributions from just the $2 \rightarrow 2$ and $2 \rightarrow 3$ core excitations, showing the importance of the different processes in Eqs. (1) and (2). Our MCBP DR rate coefficient for $2 \rightarrow 2$ excitation agrees closely

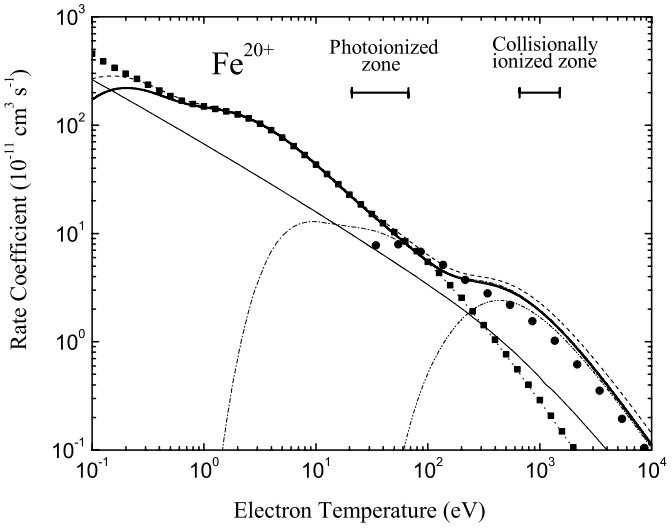

Fig. 2. Maxwellian-average DR rate coefficients for Fe^{20+} as a function of electron temperature (in eV). The *thick solid curve* represents our MCBP calculations, the *solid squares* represent the experimentally derived rate coefficients for just the $2 \rightarrow 2$ core excitations (Savin et al. 2003). Also shown are our contributions due to just the $2 \rightarrow 2$ core excitations (dotted line), the $2 \rightarrow 3$ core excitations (dash-dot-dotted line), and RR (thin solid curve). Comparison is given with the LS-coupling calculations of Jacobs et al. (1977, solid circles), the unpublished LS-calculations of Roszman as given by Arnaud & Raymond (1992, dot-dashed curve), and the recent calculations of Gu (2003, short-dashed curve). For reference we have plotted up the temperature ranges where Fe^{20+} is predicted to form in photoionization equilibrium (Kallman & Bautista 2001) and collisional ionization equilibrium (Gu 2003).

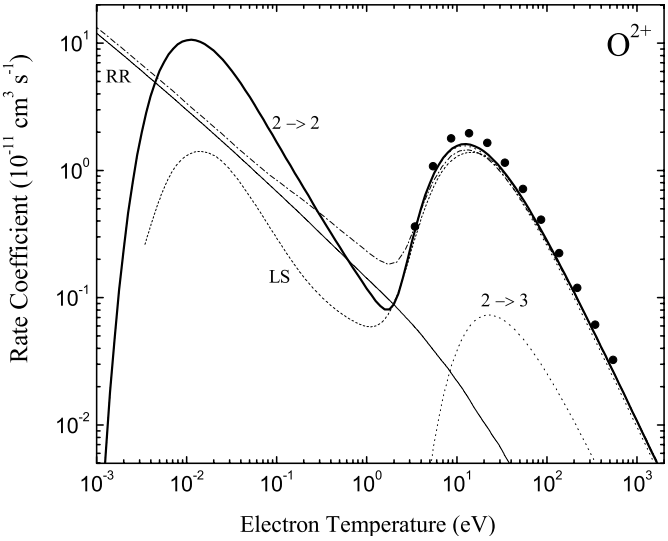

Fig. 3. Maxwellian-average $2 \rightarrow 2$ DR rate coefficients for O^{2+} as a function of electron temperature (in eV). The thick solid curve represents our MCBP IC results and the dashed curve represents our LS-coupling results. Comparison is made with the MCBP results of Badnell & Pindzola (1989, solid circles) and DR+RR LS R-matrix results of Nahar (1999, dot-dashed curve). Also shown are our contributions due to just the $2 \rightarrow 2$ and $2 \rightarrow 3$ core excitations (dotted curves – the $2 \rightarrow 2$ curve is barely distinguishable from the total curve) and RR (thin solid curve).

with the experimental results within the estimated experimental uncertainty of ≈20% for all temperatures except the low-temperature region below 0.3 eV. In photoionized plasmas with cosmic abundances, Fe^{20+} is predicted to form at temperatures of $k_B T_e \approx 20-80$ eV (Kallman & Bautista 2001). In an electron-ionized plasma, at equilibrium Fe^{20+} is predicted to form between $k_B T_e \approx 660-1510$ eV (Gu 2003), and in this region, the main contribution to the total DR rate coefficient comes from the $2 \rightarrow 3$ core excitation.

As seen from Fig. 2, there is a large discrepancy at low temperatures with earlier results. Those earlier calculations did not include DR contributions due to $2 \rightarrow 2$ $\Delta l = 0$ fine-structure core transitions (the first line in Eq. (1)), and thus did not reproduce correctly the low-temperature DR rate coefficient behavior. At higher temperatures, there is also a noticeable discrepancy with the simplified calculations of Jacobs et al. (1977). Closer agreement for higher temperatures is seen with the fitting data of Mazzotta et al. (1998), based on the unpublished results of Roszman as given by Arnaud & Raymond (1992). For comparison of the relative RR and DR contributions, we also show the RR rate coefficient in Fig. 2. Note also that for $Fe^{20+} 2 \rightarrow 2$ DR, excellent agreement was found between our results and the recent MCDF and FAC results presented by Savin et al. (2003). These last two calculations essentially differ from ours only by using Dirac-Fock wave functions for the target description (a more detailed comparison and discussion is given in Savin et al. 2003). We finally note that there is good agreement, for the most part, between our results and the recent results of Gu (2003), although the results of Gu start to become noticeably greater than ours at a temperature of about 30 eV, which is in the middle of the photoionized zone, and eventually become as much as ≈10% greater than ours at about 100 eV and all higher temperatures, including the collisionally ionized zone – see Fig. 2. (We are unable to explain these latter large differences.)

Our calculations have been carried out in the independent processes approximation, i.e., we neglect interference between RR and DR. It has been shown (Pindzola et al. 1992; Gorczyca et al. 1996) that interference effects have generally only a very small effect on the total (and strongest partial) rate coefficients. This is also true for the present case of DR on carbon-like ions, as seen by the comparison in Fig. 3 of our O^{2+} DR rate coefficients with LS-coupling R-matrix results of Nahar (1999). We see very close agreement at higher temperatures; in the low-temperature region, the difference is due to relativistic effects, which we include but the LS calculations of Nahar (1999) do not. The ^{3}P ground term is spin-orbit split into three levels (see Eq. (1)), and this splitting creates additional DR channels, leading to a significant increase in the total low-temperature DR rate coefficient. For higher temperatures, core fine-structure interactions lead to a small increase of rate coefficient (no more than 10%). The ≈15% difference with the earlier calculations of Badnell & Pindzola (1989) we attribute to the use of different atomic orbitals. Note also that at this lower charge state, the $2 \rightarrow 3$ contribution is much smaller than the $2 \rightarrow 2$ contribution.

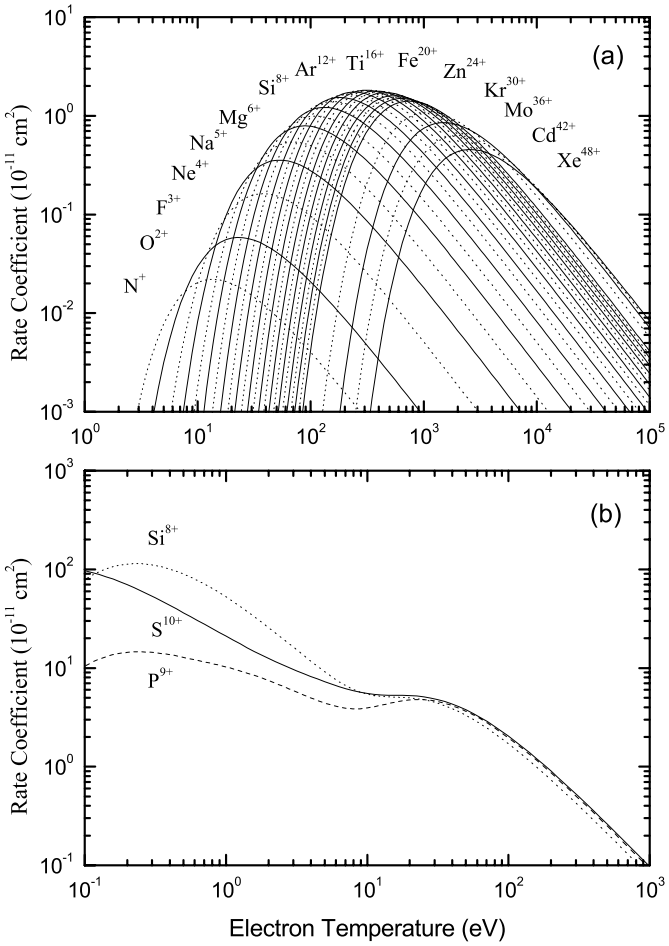

Fig. 4. Behavior of carbon-like DR rate coefficients as a function of atomic number. **a)** Total DR rate coefficients for $2 \rightarrow 3$ DR for C-like N through Zn, as well as Kr, Mo, Cd, and Xe are shown. Not all ions are labeled. **b)** Total $2 \rightarrow 2$ DR rate coefficient for Si^{8+}, P^{9+}, and S^{10+} showing irregular Z-dependence in the low temperature rate coefficient.

In Table 1, we present the fitting parameters for total DR rate coefficients for each ion from N^+ to Zn^{24+}, and also for the highly-charged ions Kr^{30+}, Mo^{36+}, Cd^{42+} and Xe^{48+}. In previous works, numerical calculations were performed for only certain selected ions, and the DR rate coefficients for the other ions were interpolated (or extrapolated) assuming smooth behavior of DR rate coefficient as a function of nuclear charge. However, we have found that such analytic interpolation formula are only applicable for the $2 \rightarrow 3$ DR rate coefficients (see Fig. 4a). The $2 \rightarrow 2$ DR rate coefficients, on the other hand, behave rather irregularly at lower temperatures, not acting smoothly as a function of Z (see Fig. 4b). The irregular behavior of the $2 \rightarrow 2$ DR rate coefficient is explained by the fact that autoionizing levels that are just above threshold for one value of Z can move just below threshold for a neighboring $Z+1$ member of the series, becoming a bound state and not contributing to DR.

An additional comparison of the earlier theoretical predictions with our results is given in Fig. 5. In the high-temperature region, we found good agreement with the simplified calculations of Jacobs et al. (1977, 1979). However, the results from the critical compilation of Mazzotta et al. (1998) are about 20–25% greater than our results. All previous calculations failed to predict the large DR rate coefficient at small temperatures due to the neglect of contributions from the fine-structure ($2p_{1/2}-2p_{3/2}$) excitation of the recombining ions. We note that, again, there is fairly good agreement between our results and the recent results of Gu (2003) except at very low energies, where presumably the slight differences in DR resonance positions manifest themselves greatly in the computed rate coefficients.

Since DR from initial metastable states is also produced here, we show selected examples of DR rate coefficients from the initial ground and metastable states $2p^2\ ^3P_{0,1,2}$, $^1D_2$ and $^1S_0$ in Fig. 6. We see that the rate coefficients for different initial terms are quite different at small temperatures. This can be explained by the different contributions from each process indicated in Eq. (1).

4. Summary

In this paper, we have systematically calculated partial and total DR rate coefficients along the carbon-like sequence as part of an assembly of a DR database necessary for the modelling of dynamic finite-density plasmas (Badnell et al. 2003). The approximations used for generating our data have been recently validated by the fairly good agreement of DR resonance strengths and energies between our theoretical data and the $2 \rightarrow 2$ experimental results from the Test Storage Ring in Heidelberg (Savin et al. 2003) for carbon-like Fe ions. Overall, we estimate the accuracy of our predicted DR rate coefficients as within 20% for temperatures above a few eV. We note, however, that storage ring results have demonstrated that all state-of-the-art theoretical methods (e.g., MCBP, MCDF, HULLAC, R-matrix, and FAC) are not able to reproduce reliably the DR resonance strengths and energies of L-shell ions for relative collision energies $\lesssim$3 eV (e.g., Savin et al. 1999, 2002b; Schippers et al. 2001). For reliable total DR rate coefficients at plasma temperatures where these resonances play a significant role, these MCBP results need to be supplemented with storage ring measurements of the relevant resonances. Nevertheless, we have ascertained, through a careful study for the present carbon-like sequence, that uncertainties in the positions of low-lying resonances do not significantly affect the rate coefficients at the temperatures where these ions are predicted to form in either photoionized or collisionally ionized equilibrium.

We have presented selected total rate coefficients for some ions of interest and have made comparisons, where possible, with previous work. We found large disagreement with previous calculations, including the fits from the recent critical compilation of Mazzotta et al. (1998). Final-state-resolved rate coefficients have been tabulated, and these data are available in either format from the web site `http://www-cfadc.phy.ornl.gov/data_and_codes`. The total DR rate coefficients have been fitted by simple analytical formula, which will also prove of great use to astrophysical and fusion plasma modelers, and are available from our web site `http://homepages.wmich.edu/~gorczyca/drdata`.

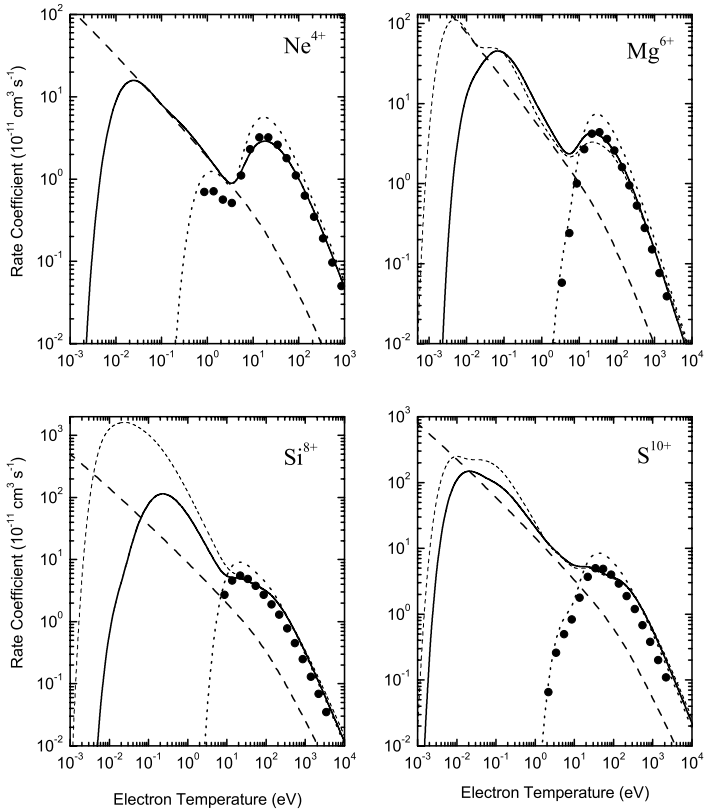

Fig. 5. Our DR (solid curve) and RR (dashed curve) rate coefficients for Ne^{4+}, Mg^{6+}, Si^{8+} and S^{10+} as compared with the early results of Jacobs et al. (1977, 1979, solid circles), the recommended data of Mazzotta et al. (1998, dotted curves), and the recent results of Gu (2003, short-dashed curve).

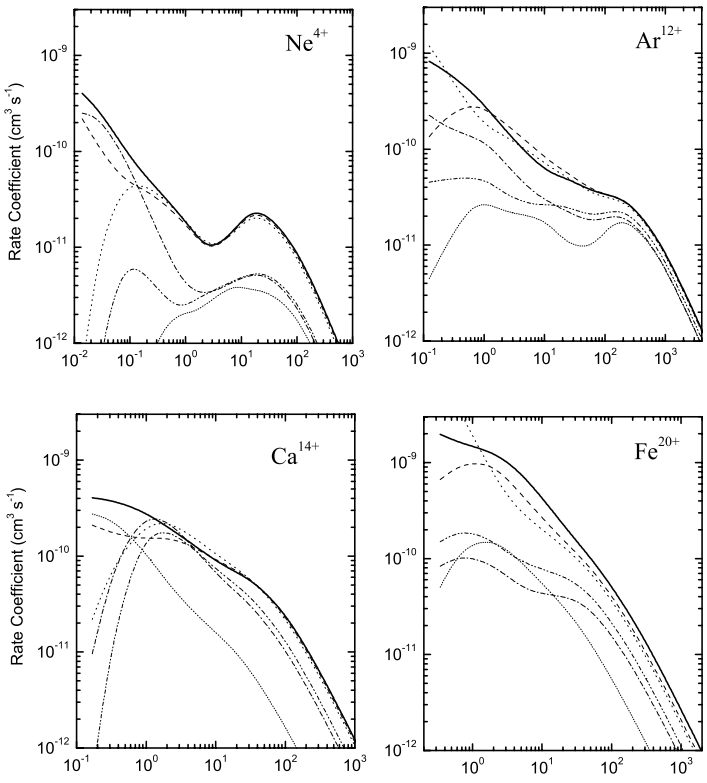

Fig. 6. Initial-state resolved DR rate coefficients as a function of electron temperature for Ne^{4+}, Ar^{12+}, Ca^{14+}, and Fe^{20+}: solid curve – $2p^2\ ^3P_0$ ground state, dashed curve – $2p^2\ ^3P_1$, coarsely dotted curve – $2p^2\ ^3P_2$, dash-dotted curve – $2p^2\ ^1D_2$, dash-dot-dotted curve – $2p^2\ ^1S_0$, finely dotted curve – $2s2p^3\ ^5S_2$ metastable state.

We have calculated our data over a wide temperature range and for a large number of atomic ions in order to maximize the available information for modelling work. Our DR fits are accurate to better than 3% for all ions in the wide temperature range from 10^1 to 10^8 K. Our RR fits are good to better than 8% in this temperature range. These RR and DR data are suitable for modelling of solar and cosmic plasmas under conditions of collisional ionization equilibrium, photoionization equilibrium, and non-equilibrium ionization. In the future, we will present dielectronic and radiative recombination data for further isoelectronic sequences as detailed previously (Badnell et al. 2003).

Acknowledgements. T.W.G., K.T.K., and O.Z. were supported in part by NASA Space Astrophysical Research and Analysis Program grant NAG5-10448. DWS was supported in part by NASA Space Astrophysics Research and Analysis Program grants NAG5-5261 and NAG5-5420 and NASA Solar Physics Research, and Subordinal Program grants NAG5-9581 and NAG5-12798.

References

Arnaud, M., & Raymond, J. 1992, ApJ, 398, 394
Badnell, N. R. 1986, J. Phys. B, 19, 3827
Badnell, N. R. 1997, J. Phys. B, 30, 1
Badnell, N. R., & Pindzola, M. S. 1989, Phys. Rev. A, 39, 1690
Badnell, N. R., O'Mullane, M. G., Summers, H. P., et al. 2003, A&A, 406, 1151 (Paper I of this series)
Burgess, A. 1965, ApJ, 205, L105
Colgan, J., Pindzola, M. S., Whiteford, A. D., & Badnell, N. R. 2003, A&A, 412, 597 (Paper III of this series)
Froese Fisher, C. 1991, Comput. Phys. Commun., 64, 369
Gorczyca, T. W., Robicheaux, F., Pindzola, M. S., & Badnell, N. R. 1995, Phys. Rev. A, 52, 3852
Gorczyca, T. W., Robicheaux, F., Pindzola, M. S., & Badnell, N. R. 1996, Phys. Rev. A, 54, 2107
Gorczyca, T. W., Badnell, N. R., & Savin, D. W. 2002, Phys. Rev. A, 65, 062707
Gu, M. F. 2003, ApJ, 590, 1131
Jacobs, V. L., Davis. J., Kepple, P. C., & Blaha, M. 1977, ApJ, 211, 605; Jacobs, V. L., Davis. J., Kepple, P. C., & Blaha, M. 1977, ApJ, 215, 690
Jacobs, V. L., Davis, J., & Rogerson, J. E. 1978, J. Quant. Spectrosc. Radiat. Transfer, 19, 591
Jacobs, V. L., Davis, J., Kepple, P. C., & Blaha, M. 1979, ApJ, 230, 627
Jacobs, V. L., Davis, J., Rogerson, J. E., et al. 1980, ApJ, 239, 1119
Kallman, T. R., & Bautista, M. A. 2001, ApJS, 133, 221
Mazzotta, P., Mazzitelli, G., Colafrancesco, S., & Vittorio, N. 1998, A&AS, 133, 403
Nahar, S. N., & Pradhan, A. K. 1997, ApJS, 111, 339
Nahar, S. N. 1999, ApJS, 120, 131
Pindzola, M. S., Badnell, N. R., & Griffin, D. C. 1992, Phys. Rev. A, 46, 5725
Ramirez, J. M., & Bautista, M. 2002, J. Phys. B, 35, 4139
Savin, D. W., Bartsch, T., Chen, M. H., et al. 1997, ApJ, 489, L115
Savin, D. W., Kahn, S. M., Linkemann, J., et al. 1999, ApJS, 123, 687
Savin, D. W. 2000, ApJ, 533, 106
Savin, D. W., & Laming, J. M. 2002, ApJ, 566, 1166
Savin, D. W., Kahn, S. M., Linkemann, J., et al. 2002a, ApJ, 576, 1098
Savin, D. W., Behar, E., Kahn, S. M., Gwinner, G., et al. 2002b, ApJS, 138, 337
Savin, D. W., Kahn, S. M., Gwinner, G., et al. 2003, ApJS, 147, 421
Summers, H. P. 2003, Atomic Data & Analysis Structure User Manual (Version 2.4) – `http://adas.phys.strath.ac.uk`
Verner, D. A., & Ferland, G. J. 1996, Astrophys. J. Suppl., 103, 467
Zatsarinny, O., Gorczyca, T. W., Korista, K. T., & Savin, D. W. 2003, A&A, 412, 587 (Paper II of this series)